Published OnlineFirst February 13, 2014; DOI: 10.1158/1535-7163.MCT-13-0858

Small Molecule Therapeutics

Molecular Cancer Therapeutics

Preclinical Evaluation of AMG 925, a FLT3/CDK4 Dual Kinase Inhibitor for Treating Acute Myeloid Leukemia

Kathleen Keegan, Cong Li, Zhihong Li, Ji Ma, Mark Ragains, Suzanne Coberly, David Hollenback, John Eksterowicz, Lingming Liang, Margaret Weidner, Justin Huard, Xianghong Wang, Grace Alba, Jessica Orf, Mei-Chu Lo, Sharon Zhao, Rachel Ngo, Ada Chen, Lily Liu, Timothy Carlson, Christophe Quéva, Lawrence R. McGee, Julio Medina, Alexander Kamb, Dineli Wickramasinghe, and Kang Dai

Abstract

Acute myeloid leukemia (AML) remains a serious unmet medical need. Despite high remission rates with chemotherapy standard-of-care treatment, the disease eventually relapses in a major proportion of patients. Activating Fms-like tyrosine kinase 3 (FLT3) mutations are found in approximately 30% of patients with AML. Targeting FLT3 receptor tyrosine kinase has shown encouraging results in treating FLT3-mutated AML. Responses, however, are not sustained and acquired resistance has been a clinical challenge. Treatment options to overcome resistance are currently the focus of research. We report here the preclinical evaluation of AMG 925, a potent, selective, and bioavailable FLT3/cyclin-dependent kinase 4 (CDK4) dual kinase inhibitor. AMG 925 inhibited AML xenograft tumor growth by 96% to 99% without significant body weight loss. The antitumor activity of AMG 925 correlated with the inhibition of STAT5 and RB phosphorylation, the pharmacodynamic markers for inhibition of FLT3 and CDK4, respectively. In addition, AMG 925 was also found to inhibit FLT3 mutants (e.g., D835Y) that are resistant to the current FLT3 inhibitors (e.g., AC220 and sorafenib). CDK4 is a cyclin D–dependent kinase that plays an essential central role in regulating cell proliferation in response to external growth signals. A critical role of the CDK4–RB pathway in cancer development has been well established. CDK4-specific inhibitors are being developed for treating RB-positive cancer. AMG 925, which combines inhibition of two kinases essential for proliferation and survival of FLT3-mutated AML cells, may improve and prolong clinical responses. *Mol Cancer Ther; 13(4); 880–9. ©2014 AACR.*

Introduction

Acute myeloid leukemia (AML) represents a significant unmet medical need. It is a hematologic malignancy characterized by uncontrolled proliferation of the hematopoietic progenitor cells of myeloid lineage. The current standard of care is chemotherapy with and without allogeneic stem cell transplantation. Induction chemotherapy is successful in 65% of all patients with AML. Using chemotherapy as consolidation, up to 50% of patients that receive consolidation go into long-term remission. The actual chance of long-term remission depends on specific prognostic factors as age, chromosomal aberrations, and molecular changes. The relative 5-year survival rate is 24% in patients diagnosed with AML (1). More efficacious and safer therapeutics are being developed and tested in clinical trials.

FLT3 (Fms-like tyrosine kinase 3) is a well-recognized drug target for treating AML. Activating mutations in FLT3 are found in approximately 30% of patients with AML (2–4). The majority of the activating mutations are internal tandem duplications (ITD) in the juxtamembrane region. Numerous FLT3 inhibitors have entered clinical studies and shown initial clinical responses. However, the responses are transient and resistance develops rapidly (5, 6). The major resistance mechanism seems to be acquisition of secondary mutations in FLT3, which interfere with the ability of small-molecule inhibitors to bind to FLT3 (4, 5). One strategy to overcome resistance to FLT3 inhibitors in the clinic is to combine them with chemotherapy despite the recognition that chemotherapy is poorly tolerated (6, 7).

Cyclin-dependent kinase 4 (CDK4) and 6 (CDK6) are two functionally indistinguishable cyclin D–dependent kinases. As a key downstream effector of growth factor activation, CDK4 promotes G_1–S transition of the cell cycle by phosphorylating the retinoblastoma protein (RB), a tumor-suppressor protein. A large body of evidence supports important involvement of the $p16^{INK4a}$-CDK4–RB axis in cancer development (8–12). RB negatively regulates the cell cycle at G_1 by sequestering E2F proteins

Authors' Affiliation: Amgen Discovery Research, Amgen Inc., One Amgen Center Drive, Thousand Oaks, California

Note: Supplementary data for this article are available at Molecular Cancer Therapeutics Online (http://mct.aacrjournals.org/).

Corresponding Author: Kang Dai, Amgen Inc., 1120 Veterans Blvd., South San Francisco, CA 94080. Phone: 650-244-2558; Fax: 650-837-9423; E-mail: kdai@amgen.com

doi: 10.1158/1535-7163.MCT-13-0858

Published OnlineFirst February 13, 2014; DOI: 10.1158/1535-7163.MCT-13-0858

that are required for initiation of S phase. $p16^{INK4a}$ is a member of the INK4 family of CDK4 cellular inhibitors (10–13) and a tumor suppressor. The genes for RB and $p16^{INK4a}$ are frequently deleted or silenced in various types of cancer. Although mutations in RB and $p16^{INK4a}$ are rare in patients with AML, $p15^{INK4b}$, another member of the INK4 family, has been reported to be downregulated in up to 60% of patients with AML (14, 15), indicating an important role of CDK4 in AML. Recently, a selective CDK4 inhibitor PD 0332991 has entered clinical trials and showed promising anticancer efficacy in patients with advanced breast cancer (16, 17). Anticancer activity of PD 0332991 has also been reported in clinical and preclinical studies of other cancer types, including AML (18–21). Here, we report the preclinical evaluation of a FLT3/CDK4 dual kinase inhibitor AMG 925. We believe that combined inhibition of two essential kinases by AMG 925 has potential to reduce development of drug resistance in patients with AML.

Materials and Methods

Compounds

AMG 925 (2-(2-((9-(trans-4-methylcyclohexyl)-9H-pyrido[4′,3′:4,5]pyrrolo[2,3-d]pyrimidin-2-yl)amino)-7,8-dihydro-1,6-naphthyridin-6(5H)-yl)-2-oxoethanol) was synthesized at Amgen. PD 0332991 and sorafenib were purchased from AdooQ BioScience.

Cell lines

MOLM13 and Mv4-11 were obtained from the DSMZ German Collection of Microorganisms and Cell Cultures. MOLM13-Luc cells were constructed by transduction of MOLM13 cells with the pLV218G luciferin/lentivector, which expresses luciferase under the murine EF1α promoter. Sorafenib-resistant MOLM13 (MOLM13sr) and Mv4-11 (Mv4-11sr) were isolated by passaging the cells in growth medium containing increasing concentrations of sorafenib (1–1,000 nmol/L). RNA was isolated from independent clones and sequenced to identify FLT3 kinase domain mutations, D835Y in MOLM13sr and D835V in Mv4-11. The other cell lines used in this study were purchased from American Type Culture Collection. Growth conditions recommended by the providers were followed. All of the cell lines were authenticated by short tandem repeat DNA profiling; MDA-MB-435, MDA-MB-436, and MDA-MB-468 were by Genetica DNA Laboratories; and the rest by DDC Medical.

Kinases

CDK4/cyclin D1, CDK6/cyclin D1, CDK1/Cyclin B, and CDK2/Cyclin A were purchased from Cell Signaling Technology. For the kinase assays, RB fragment (amino acids 773–928) and histone H1 (Millipore) were used as substrate for CDK4/6 and CDK1/2, respectively. [r-^{33}P]-ATP was from PerkinElmer. The assays were performed in 96-well filter plates (MSDVN6B50; Millipore) with a final volume of 100 μL, containing 1 μg RB, 25 ng CDK4/cyclin D1, 25 μmol/L ATP, 1 μCi [r-^{33}P]-ATP, and the test compound in kinase reaction buffer (20 mmol/L Tris-HCl, pH 7.4, 10 mmol/L $MgCl_2$, 5 mmol/L β-glycerophosphate, 1 mmol/L dithiothreitol (DTT), and 0.1% bovine serum albumin). The reaction mixes were incubated at room temperature for 1 hour and terminated with 20% trichloroacetic acid (TCA). Wells were washed with 10% TCA, let dry, and processed for scintillation counting with TopCount (PerkinElmer). FLT3 kinase assay was performed using a time-resolved fluorescence resonance energy transfer assay. The FLT3 enzyme (glutathione S-transferase–fused human FLT3 cytoplasmic domain, amino acids 564–993) was from Carna Biosciences. An ULight-labeled synthetic peptide (ULight-JAK1; PerkinElmer) derived from human Janus kinase 1 (amino acids 1015–1027) was used as the phosphoacceptor substrate. The FLT3 kinase reaction was conducted in a 384-well white OptiPlate (PerkinElmer) in a total volume of 20 μL. The reaction mixture contained 50 nmol/L ULight-JAK1, 116 μmol/L ATP (equal to K_m), 0.5 nmol/L FLT3, and serially diluted test compounds in a reaction buffer of 50 mmol/L Hepes, pH 7.6, 1 mmol/L EGTA, 10 mmol/L $MgCl_2$, 2 mmol/L DTT, and 0.005% Tween 20. The reaction was allowed to proceed for 1 hour at room temperature and stopped by adding 20 μL of 20 mmol/L EDTA and 4 nmol/L LANCE Eu-W1024 anti-phosphotyrosine antibody in LANCE detection buffer (PerkinElmer). The plates were incubated at room temperature for 2 hours after addition of detection reagents and were then read on an Envision multimode reader (PerkinElmer). Fluorescence signals were measured at 615 nm (8.5-nm bandwidth) and 665 nm (7.5-nm bandwidth) with a 60-μs delay after excitation at 320 nm (75-nm bandwidth). The signal ratio at 665/615 nm was used in all data analyses.

Cell growth, apoptosis, and cell cycle

Cell growth was measured by a DNA synthesis assay. Cells were seeded in a 96-well Cytostar T plate (GE Healthcare Biosciences) at a density of 5×10^3 cells/well in a total volume of 160 μL. Test compounds were serially diluted into the plate (20 μL/well) and 20 μL/0.1 μCi of [^{14}C]-Thymidine (GE Healthcare Biosciences) added to each well. Isotope incorporation was determined using a β plate counter (Wallac) after further 72-hour incubation. Apoptosis was assayed by using the Vybrant Apoptosis Assay Kit#9 (Invitrogen; Cat# V35113) following the manufacturer's protocol. Briefly, cells were seeded into a 6-well plate at 5×10^5 cells per well and treated with compounds for 24 hours. The cells were then stained with reagents provided in the kit and analyzed by flow cytometry. The Sytox Green fluorescence versus allophycocyanin fluorescence dot plot shows resolution of live, apoptotic, and dead cells, which were quantified using the Flowjo software. The cell-cycle analysis was done by treating the cells with AMG 925 for 24 hours followed by using the CycleTest Kit (BD Biosciences) following manufacturer's instructions. Ten thousand events were acquired and the

Published OnlineFirst February 13, 2014; DOI: 10.1158/1535-7163.MCT-13-0858

proportions of cells in each cycle phase were calculated using the ModFit software.

P-FLT3, P-STAT5, and P-RB

Phospho-FLT3 (P-FLT3) was determined by immunoprecipitation and Western blotting (IP-WB). A total of 2×10^7 cells/mL were treated with compounds for 1 hour. Cell lysates were prepared in RIBA cell lysis buffer (G-Biosciences; Cat# 786-489) incubated with an anti-FLT3 antibody (Cell Signaling Technology; Cat# 3462) at 4°C overnight. Immunocomplexes were recovered with the Protein G Kit (Sigma; Cat# 087K4817) and subjected to WB with anti-phosphotyrosine 4G10 (Millipore; Cat# 05-1050) for P-FLT3 or an anti-FLT3 antibody (R&D Systems; Cat# BAF812) for total FLT3 (T-FLT3). Protein bands were visualized using enhanced chemiluminescence reagents (GE Healthcare Bio-Sciences; Cat# RPN2106) and analyzed with the ImageJ software (NIH). Meso Scale Discovery (MSD) assays were used to determine cellular levels of phospho-STAT5 (P-STAT5) and phospho-RB (P-RB). A total of 1×10^4 cells/well in 96-well plates were incubated with dilutions of compounds. Cell lysates were harvested 1 or 24 hours after addition of compounds for determination of P-STAT5 and P-RB, respectively, using kits from Meso Scale Discovery (Cat# K150IGD-1 for P-STAT5 and Cat# K150ITD-1 for P-RB).

To determine P-STAT5 or P-RB in xenograft tumor samples, tumors were allowed to grow to 200 to 250 mm^3 before administration of AMG 925 via oral gavages. The tumor samples were dissected and snap frozen at different time points after dosing, and the lysates prepared and assayed for levels of P-STAT5 and P-RB similarly as for cultured cells.

MOLM13 xenograft tumor model

CrTac:NCR-*Foxn1*^{nu} (NCR) nude mice were treated with an intraperitoneal (i.p.) injection of 100 μL of anti-asialo GM (WAKO Chemicals) antibody to abolish natural killer activity and allow for enhanced growth of subsequently inoculated tumor cells. The following day, 7.5 million MOLM13 tumor cells in PBS were formulated as a 1:1 mixture with Matrigel (BD Biosciences) and injected into the subcutaneous space on the right flank of the mice. Tumors were measured with PRO-MAX electronic digital caliper (Japan Micrometer Mfg. Co. LTD) and the mice were weighed every other day before each tumor measurement. Tumor volumes were calculated as follows: tumor volume (mm^3) = $[(W^2 \times L)/2]$ in which width (W) is defined as the smaller of the two measurements and length (L) is defined as the larger of the two measurements.

MOLM13-Luc systemic tumor model

MOLM13-Luc cells stably expressing luciferase were injected intravenously (i.v.) into NOD/SCID IL-2Rγ$^{-/-}$ (NSG) mice. After 6 days, mice were injected with an i.p. injection of D-luciferin, tissues removed, and imaged using an IVIS imager. MOLM13-Luc cells localized to the spleen and the bone marrow of the sternum and hind limbs. At 13 days after injection, tumor cells were more widespread to the peripheral blood, spleen, lung, ovaries, and calvaria. For efficacy evaluation of AMG 925, 5×10^4 MOLM13-Luc cells in PBS were inoculated via i.v. injection in tail vein. The cells were allowed to grow for 6 days and randomized for treatment using imaging with a Xenogen IVIS 200 imager (PerkinElmer). Before imaging, mice were given an i.p. injection of 150 mg/kg Firefly D-luciferin (Caliper Life Sciences) and dorsal and ventral images were captured. Tumor burden was quantified using Living Image 2.5 software for regions of interest (ROI): total body (dorsal and ventral). Mice ($n = 60$) were sorted from low to high by drawing ROIs over the dorsal and ventral images and taking the sum of these images (whole-body bioluminescence imaging). The bottom 5 and top 5 animals in the sort were excluded from the study. The remaining mice were randomly assigned to therapeutic groups to achieve five groups of ($n = 10$) with equivalent whole-body tumor burden. Treatments were initiated on day 7 and continued for 10 consecutive days. Twice daily doses were administered 6 hours apart. After completion of the treatments, mice were monitored for either development of hind limb paralysis (HLP) that resulted from disease progression and >20% body weight loss. Mice were humanely sacrificed using CO_2 asphyxiation and cervical dislocation in accordance with Amgen Institutional Animal Care and Use Committee (IACUC) criteria.

Colo205 xenograft tumor model

2×10^6 cells were innoculated on the flank of NCR nude mice and allowed to grow for 13 days. Mice were then dosed twice a day by oral administration 6 hours apart with 12.5, 25, 37.5, and 50 mg/kg of AMG 925 formulated in 2% hydroxypropyl methylcellulose/1% Tween 80 for 10 consecutive days.

Pharmacokinetics and plasma concentration

Animals were orally dosed with AMG 925 and plasma samples were collected at time points after dosing. Concentrations of AMG 925 in the plasma were determined with a multiple reaction monitoring method on a triple quadrupole mass spectrometer coupled with high-pressure liquid chromatography system. Unbound AMG 925 concentrations were calculated based on protein binding of the compound.

Immunohistochemistry

Femur samples from 3 mice in each of the treatment groups were taken at 2 and 18 hours after the last dose and processed for cutting sections for immunohistochemistry (IHC) staining. Sections were deparaffinized and then heated in DIVA Decloaker solution for P-RB (Biocare) or BORG Decloaker for P-STAT5 (Biocare) for 1 hour for antigen retrieval. Remaining IHC steps were performed at room temperature in a DAKO Autostainer. Sections were incubated for 10 minutes with Peroxidazed 1 (Biocare) to block endogenous peroxidase, followed by incubation for 10 minutes with Background Sniper for P-RB

Published OnlineFirst February 13, 2014; DOI: 10.1158/1535-7163.MCT-13-0858

(Biocare) or 10% normal goat serum in rodent block M for P-STAT5 to reduce nonspecific background. Sections were then incubated for 1 hour with FITC-P-RB at 0.375 μg/mL or P-STAT5 antibodies (Cell Signaling Technology) at 3.26 μg/mL, and incubated for 30 minutes with rabbit anti-FITC immunoglobulin G 1:200 (Invitrogen) for FITC-P-RB. Sections were incubated for 30 minutes with Envision+ HRP (horseradish peroxidase) anti-rabbit polymer (DAKO), followed by DAB+ (DAKO) for 5 minutes. Sections were counterstained with hematoxylin (DAKO) for approximately 1 minute. Ten 40× fields (720 × 720 pixels) of MOLM13-Luc tumor cells were then counted for the presence of positive staining nuclei. A nucleus was considered positive if it had uniform staining of at least "1+" intensity. Average fraction positive P-STAT5 and P-RB were then calculated for each field and treatment group medians and significance were generated by GraphPad calculator with an unpaired *t* test and two-tailed *P* values.

Statistical analysis and IC_{50} determination

Tumor volumes are expressed as means ± SE and plotted as a function of time. Statistical significance of observed differences between growth curves was evaluated by repeated measures analysis of covariance of the log transformed tumor volume data with Dunnett-adjusted multiple comparisons. The analysis was done using SAS proc mixed with model effects of baseline log tumor volume, day, treatment, and day-by-treatment interaction; a repeated statement in which day was a repeated value, animal the subject, and a Toeplitz covariance structure; and an lsmeans statement to do a Dunnett analysis comparing the control group with the other treatment groups. All statistical calculations were made through the use of JMP software v7.0 interfaced with SAS v9.1 (SAS Institute, Inc.). For the Kaplan–Meier analysis in the systemic AML mouse model, the statistical analysis was performed using the log-rank test using JMP software v7.0 interfaced with SAS v9.1 (SAS Institute, Inc.). A difference between groups was deemed significant if $P < 0.05$. IC_{50} values of AMG 925 in *in vitro* assays were determined by nonlinear regression curve fitting using GraphPad Prism v5.01 (GraphPad).

Results

AMG 925 is a potent, selective, and orally available FLT3/CDK4 dual inhibitor

AMG 925 was discovered by high throughput screening and lead optimization. *In vitro* activities of AMG 925 are summarized in Table 1 and Fig. 1. AMG 925 potently inhibited FLT3, CDK4, and CDK6 in kinase assays with IC_{50} in single-digit nanomolar range. The selectivity of AMG 925 for CDK4 and FLT3 against CDK1, in which inhibition is highly cytotoxic, was >500-fold. A fair overall kinase selectivity of AMG 925 was as determined by KinomScan against a panel of 442 various kinases (Supplementary Table S1). Cellular selectivity (on-target vs. off-target activity) of AMG 925 was about 50-fold as evaluated by comparison of its growth-inhibiting activity in RB-positive (RB^+) and RB-negative (RB^-) non-AML cancer cell lines (Table 1).

Table 1. *In vitro* activities of AMG 925

Kinase assays IC_{50}, μmol/L	
FLT3	0.002 ± 0.001
CDK4	0.003 ± 0.001
CDK6	0.008 ± 0.002
CDK1	1.90 ± 0.51
CDK2	0.375 ± 0.15
Cellular assays IC_{50}, μmol/L	
Growth inhibition	
MOLM13 (FLT3-ITD)	0.019 ± 0.006
Mv4-11 (FLT3-ITD)	0.018 ± 0.004
U937 (FLT3-WT)	0.052 ± 0.013
THP1 (FLT3-WT)	0.047 ± 0.011
MOLM13sr (FLT3-ITD/D835Y)	0.023 ± 0.010
Mv4-11sr (FLT3-ITD/D835V)	0.009 ± 0.005
Colo205 (RB^+)	0.055 ± 0.009
MDA-MB-435 (RB^+)	0.034 ± 0.008
MDA-MB-436 (RB^-)	2.0 ± 0.7
MDA-MB-468 (RB^-)	2.8 ± 0.7
P-STAT5	
MOLM13 (FLT3-ITD)	0.005 ± 0.003
Mv4-11 (FLT3-ITD)	0.004 ± 0.005
MOLM13sr (FLT3-ITD/D835Y)	0.026 ± 0.011
Mv4-11sr (FLT3-ITD/D835V)	0.015 ± 0.008
U937 (FLT3-WT)	>3
P-RB	
MOLM13	0.009 ± 0.004
Colo205	0.023 ± 0.006

NOTE: Relevant genotypes of cell lines are shown in parentheses. Experiments to determine IC_{50} were repeated at least 3 times. IC_{50} values indicated as mean ± SD.
Abbreviation: Mv4-11sr, sorafenib-resistant Mv4-11.

AMG 925 potently inhibited growth of AML cell lines MOLM13 (FLT3-ITD; $IC_{50} = 0.019$ μmol/L) and Mv4-11 (FLT3-ITD; $IC_{50} = 0.018$ μmol/L). To determine that AMG 925 inhibited growth of MOLM13 and Mv4-11 cells through FLT3, P-FLT3 and P-STAT5, direct substrates of FLT3-ITD (22), were measured as specific pharmacodynamic markers. In addition, apoptosis, a phenotype characteristic of inhibition of FLT3 in sensitive AML cells, was examined. As shown in Table 1, AMG 925 potently inhibited P-STAT5 in AML cell lines MOLM13 (FLT3-ITD) and Mv4-11 (FLT3-ITD) with IC_{50} values comparable with those for kinase and growth inhibition. In Fig. 1B, AMG 925 induced apoptosis in MOLM13 in a dose-dependent manner, but not in the FLT3-independent U937, indicating a specific inhibition of FLT3 in MOLM13. Furthermore, the apoptosis correlated with inhibition of P-FLT3 and P-STAT5 in treated cells. Similar effects by AMG 925 were observed in Mv4-11 cells (data not shown). To demonstrate inhibition of CDK4 by AMG 925 in cells, cell-cycle analysis was carried. As shown in Fig. 1C, AMG

Published OnlineFirst February 13, 2014; DOI: 10.1158/1535-7163.MCT-13-0858

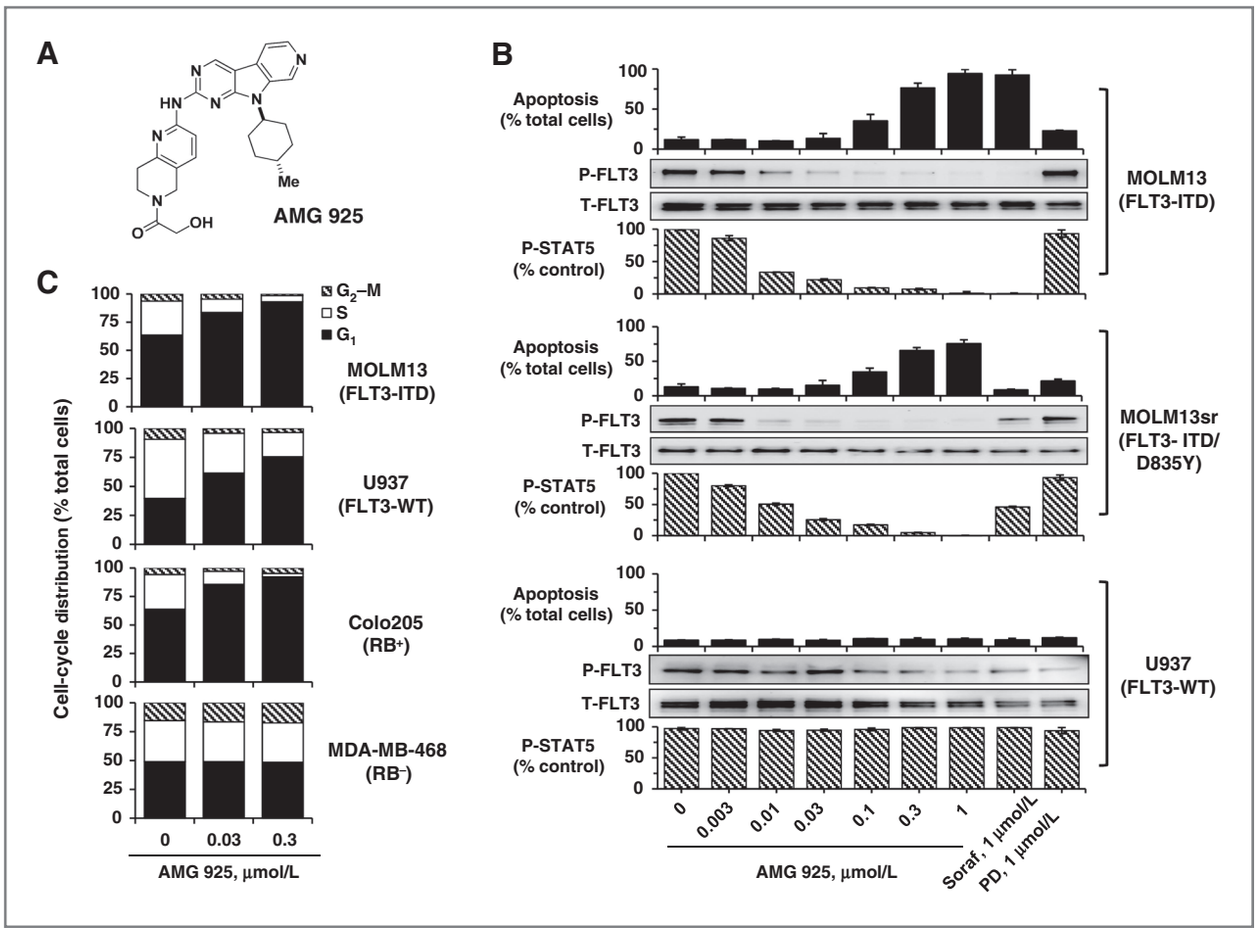

Figure 1. AMG 925 induced apoptosis and G_1 cell-cycle arrest in AML cells. A, structure of AMG 925. B, AMG 925 induced apoptosis in MOLM13 (FLT3-ITD) and MOLM13sr (FLT3-ITD/D835Y, sorafenib-resistant) but not in U937 (FLT3-WT) AML cells, in correlation with inhibition of P-FLT3 and P-STAT5 in the cells. MOLM13, MOLM13sr, and U937 cells were treated with AMG 925 and control compounds for 48 hours and analyzed for apoptosis by Annexin V/Sytox Green staining and flow cytometry. Levels of P-FLT3 and P-STAT5 were determined after 1 hour compound treatments by IP-WB and MSD assay, respectively. C, AMG 925 induced G_1 cell-cycle arrest in RB^+ MOLM13, U937, or Colo205 cells, but not in RB^- MDA-MB-468 cells. The cells were incubated with AMG 925 for 24 hours, fixed, and analyzed for DNA content with propidium iodide staining and flow cytometry. PD, PD 0332991 (CDK4 inhibitor); Soraf, sorafenib (FLT3 inhibitor).

925 induced G_1 arrest in RB^+ MOLM13, U937, and Colo205. In contrast, AMG 925 did not cause G_1 arrest in RB^- MDA-MB-468, which is consistent with the growth inhibition potency of AMG 925 in these cell lines (Table 1).

Pharmacokinetic analysis showed that AMG 925 was orally available with a half-life appropriate for twice daily dosing in preclinical animals (Supplementary Fig. S1).

AMG 925 inhibits signaling of FLT3-ITD/D835 mutants

Two sorafenib-resistant AML cell lines MOLM13sr and Mv4-11sr were isolated as described in Materials and Methods. The parental cells MOLM13 and Mv4-11 acquired FLT3-D835Y and Mv4-11sr FLT3-D835V, respectively, during isolation for resistance to sorafenib. We found that AMG 925 inhibited growth of both sorafenib-resistant AML cell lines with potency comparable with those of the parental cell lines MOLM13 and Mv4-11 (Table 1). Growth inhibition of MOLM13sr and Mv4-11sr by AMG 925 is believed to be primarily through FLT3, which is supported by potent inhibition of P-STAT5 by AMG 925 in the cells (Table 1). This is also supported by dose-dependent induction of apoptosis by AMG 925 in the MOLM13sr cells, which was correlated with inhibition of P-FLT3 and P-STAT5 (Fig. 1B). Sorafenib, however, caused only background level of apoptosis and was much less potent in inhibiting P-FLT3 or P-STAT5 than AMG 925. Similar effects were observed in Mv4-11sr (our unpublished observations).

AMG 925 inhibits growth of subcutaneous MOLM13 xenograft tumors

MOLM13 tumor–bearing mice were dosed twice daily by oral administration 6 hours apart with 12.5, 25, or 37.5

Published OnlineFirst February 13, 2014; DOI: 10.1158/1535-7163.MCT-13-0858

mg/kg AMG 925. Tumors were then harvested 3, 9, 12, and 24 hours after the first dose, and analyzed for levels of P-STAT5 and P-RB. Maximum inhibition of P-STAT5 and P-RB was achieved at 6 and 12 hours respectively at the 37.5 mg/kg dose of AMG 925 (Fig. 2A, top and bottom). Interestingly, a rebound of P-STAT5 at 24 hours was observed, possibly as a result of compensational feedback. The pharmacodynamic responses of P-STAT5 and P-RB inhibition correlated with plasma concentrations of AMG 925 (Fig. 2A, top and bottom).

To determine antitumor efficacy of AMG 925, tumor-bearing mice were orally dosed twice daily with AMG 925. Dose-dependent inhibition of tumor growth was observed with the maximum inhibition after treatment with 37.5 mg/kg AMG 925 (tumor growth inhibition, TGI = 96%; $P < 0.0001$; Fig. 2B, top). Taken together with the pharmacodynamic data, this suggests that maximal efficacy in this model was achieved with greater than 80% inhibition of P-STAT5 and greater than 90%inhibition of P-RB for at least 12 hours. No differences in body weight were observed (Fig. 2B, bottom). An ED_{50} of 9.2 mg/kg (95% confidence interval, CI, 5.8–14.4) was calculated using individual tumor volumes on day 15.

AMG 925 inhibits growth of systemic MOLM13-Luc xenograft tumors

To more closely mimic human AML, a MOLM13 systemic tumor model was developed (see Materials and Methods). Mice injected with MOLM13-Luc cells were dosed with AMG 925 twice daily for 10 consecutive days. AMG 925 demonstrated dose-dependent antitumor activity with calculated TGI of 99.7%, 97%, and 71% for the 37.5, 25, and 12.5 mg/kg dose groups, respectively (Fig. 3A). An ED_{50} of 11 mg/kg (95% CI, 9.7–12.3) was calculated, which was consistent with the ED_{50} determined in the MOLM13 subcutaneous tumor model. Figure 3B represents images taken at the end of the dosing period showing that tumor cells in mice (colored) were greatly reduced compared with vehicle control. No effects on body weight were observed during the dosing period. Time to moribund sacrifice was also measured for the systemic MOLM13-Luc tumor model. After completion of

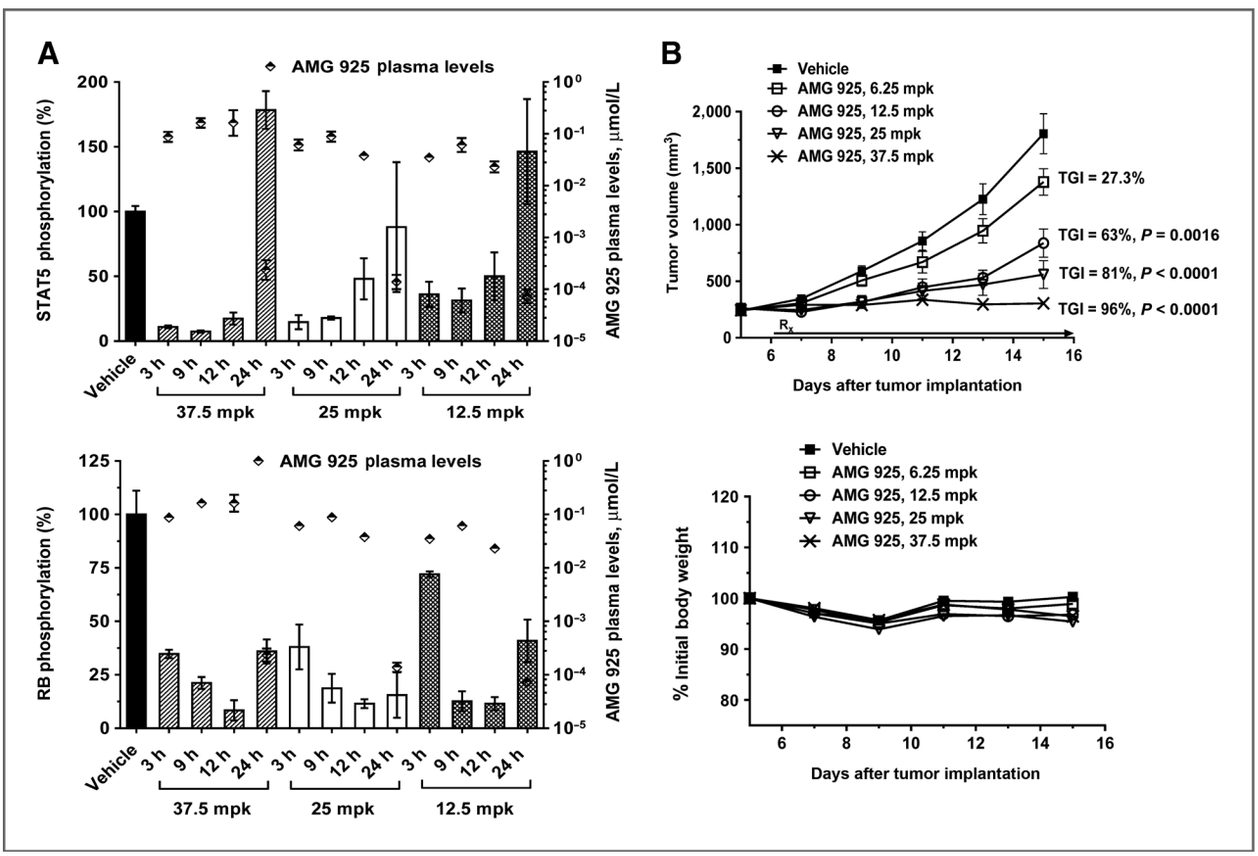

Figure 2. Activity of AMG 925 in subcutaneous MOLM13 xenograft tumor model. A, effect of AMG 925 on P-STAT5 and P-RB levels in MOLM13 xenograft tumors. Mice were administered AMG 925 at 12.5, 25, or 37.5 mg/kg (mpk). Tumors lysates were prepared and the level of P-STAT5 (top) or P-RB (bottom) was determined. Unbound plasma levels of AMG 925 (μmol/L), same time points are shown. Data, mean ± SEM; $n = 3$ except for vehicle group ($n = 6$). B, antitumor activity of AMG 925 on MOLM13 xenograft tumors. Nude mice bearing subcutaneous MOLM13 tumor ($n = 10$ per group) were treated with 6.25, 12.5, 25, or 37.5 mpk AMG 925 for 10 consecutive days and TGI was determined (top). No significant body weight changes in AMG 925–treated mice compared with vehicle were detected during the course of the treatments (bottom).

Published OnlineFirst February 13, 2014; DOI: 10.1158/1535-7163.MCT-13-0858

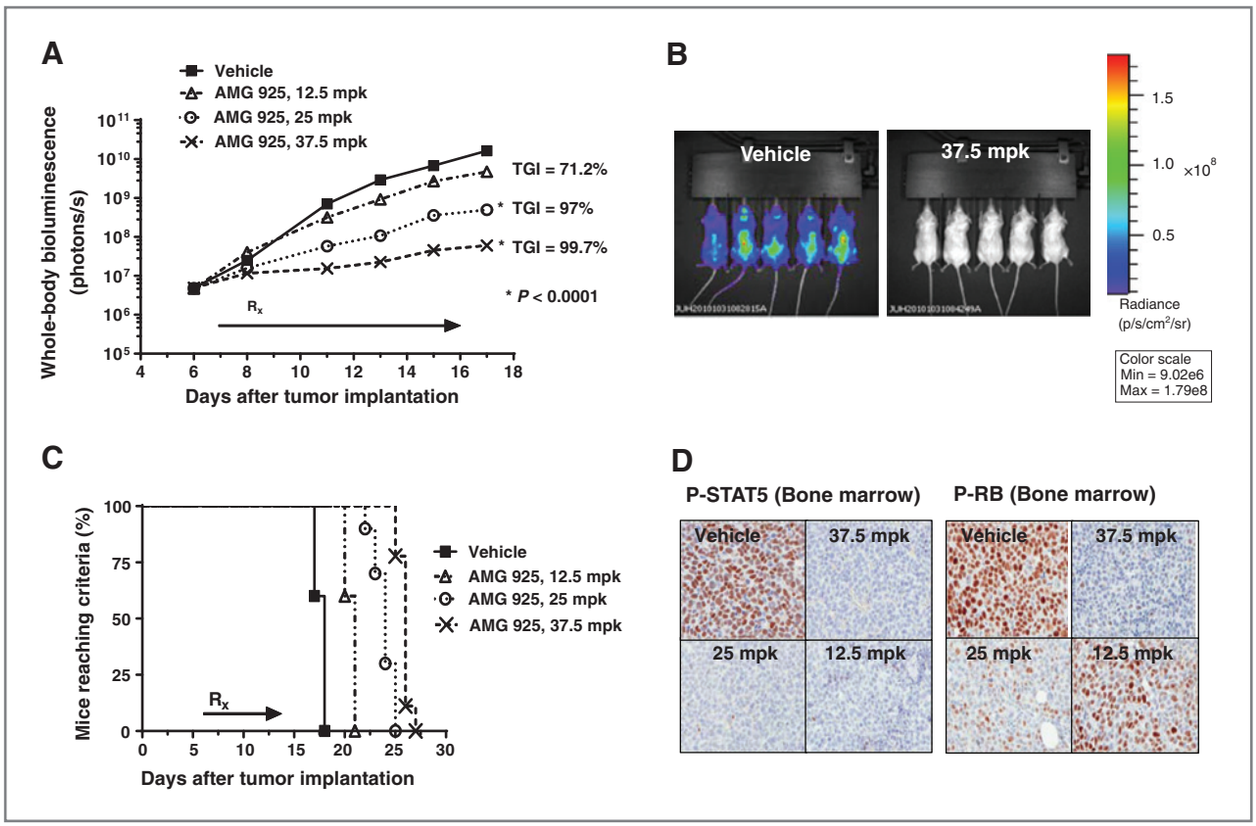

Figure 3. Activity of AMG 925 in systemic MOLM13-Luc xenograft tumor model. A, NSG mice engrafted with MOLM13-Luc tumors were treated with 12.5, 25, or 37.5 mg/kg (mpk) AMG 925. Tumor burden was determined by quantification of total body bioluminescence. Mice were injected with 150 mpk Firefly D-luciferin before imaging. Using unpaired *t* test and two-tailed *P* values to determine significance, all AMG 925 treatment groups were shown to be significant as compared with vehicle group. All comparisons with vehicle have a $P < 0.001$. B, bioluminescence images of mice at the end of dosing period. C, all AMG 925 treatments significantly increased time to humane sacrifice relative to vehicle. Mice that were moribund, showed signs of HLP, or lost 20% of starting body weight were euthanized and plotted. D, femurs of mice treated similarly as in A were harvested at 8 or 24 hours after the initial dose administration and processed for IHC staining for P-STAT5 or P-RB and positive nuclei counted (see Supplementary Fig. S2 for quantitative data).

the 10-day dosing period, mice were monitored for signs of morbidity and sacrificed according to IACUC guidance. The mean time to moribund sacrifice was 21, 24, and 26 days for the 12.5, 25, and 37.5 mg/kg doses, respectively, compared with 17.4 days for the vehicle-treated mice ($P < 0.05$; Fig. 3C). After cessation of AMG 925 treatment, all mice eventually succumbed to disease progression. The terminal symptoms of mice in all treatment groups were similar to those in the vehicle group. MOLM13-Luc cells were detectably further spread from the initial major sites of spleen and the bone marrow of sternum and hind limbs to the peripheral blood, lung, ovaries, and calvaria (Fig. 3B). HLP, which apparently resulted from severe infiltration of the AML cells in the bone of hind limbs, was closely observed as the beginning of terminal stage of the disease. As soon as the mice showed HLP and/or 20% weight loss, they were humanely sacrificed.

To correlate the antitumor activity of AMG 925 with pharmacodynamic activity in this systemic model, the effect of AMG 925 on P-STAT5 and P-RB in the bone marrow–engrafted tumor cells was assessed in a separate pharmacokinetic/pharmacodynamic analysis. Mice were injected with MOLM13-Luc cells and 14 days after injection, mice were administered two doses of AMG 925 6 hours apart. Femurs were harvested 8 and 24 hours after the first dose administration and processed for our IHC staining of P-STAT5- and P-RB–positive cells. At all doses tested, P-STAT5 was reduced to less than 3% but returned to baseline by 24 hours after dosing (Fig. 3D; Supplementary Fig. S2A). P-RB was reduced to approximately 20% at 8 and 24 hours after administration of the 37.5 mg/kg dose. At 24 hours after dosing, a dose-dependent decrease in inhibition of P-RB was observed (Fig. 3D; Supplementary Fig. S2B). These data, together with the antitumor activity, demonstrate that maximal activity of AMG 925 requires complete inhibition of STAT5 phosphorylation for at least 8 hours and 80% inhibition of RB phosphorylation for 24 hours.

TGI by AMG 925 in Colo205 xenografts

To demonstrate that the CDK4/6 inhibitory activity of AMG 925 would lead to TGI, we used the RB-positive

Published OnlineFirst February 13, 2014; DOI: 10.1158/1535-7163.MCT-13-0858

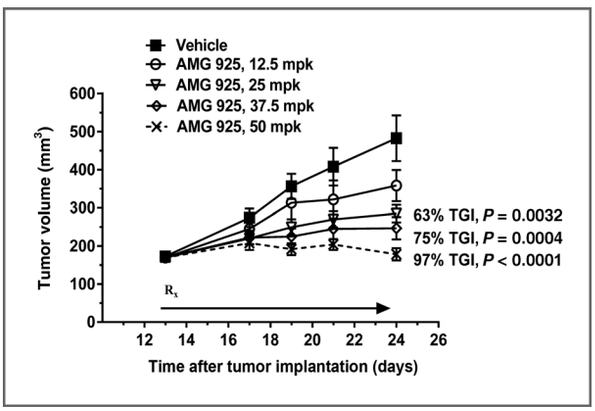

Figure 4. Activity of AMG 925 in Colo205 xenograft tumor model. Nude mice injected subcutaneously with Colo205 cells. Oral administration of AMG 925 was given at 12.5, 25, 37.5, and 50 mg/kg (mpk) twice daily, for 10 consecutive days. TGI was determined at 24 hours after the last dosing. Data, mean ± SEM.

Colo205 colon adenocarcinoma xenograft model in which growth was independent of FLT3 activity. Oral administration of AMG 925 resulted in dose-dependent antitumor activity with a TGI of 97% at the highest dose tested (50 mg/kg, twice daily; Fig. 4). The ED_{50} was calculated as 37 mg/kg (95% CI, 26–51). Body weight loss was not observed. The TGI correlated with inhibition of P-RB and plasma concentrations of AMG 925 (data not shown).

Discussion

Numerous FLT3 inhibitors and multiple receptor tyrosine kinase inhibitors with FLT3 inhibitory activity have been tested for treating AML. Despite transient responses, the disease relapses quickly, diminishing the overall clinical benefits of the FLT3 inhibitors as monotherapy (2–5). Several mechanisms have been described as contributing to relapse: (i) acquired mutations in FLT3 that interfere with inhibitor binding; (ii) increased expression of anti-apoptotic factors like Bcl-2 and Mcl-1; (iii) elevated compensatory growth factor signaling; (iv) protective microenvironment of bone marrow; and (v) insufficient FLT3 target coverage. Results from a recent phase II study of AC220, a highly potent and selective FLT3 inhibitor, provide strong evidence that acquired resistance mutations are primary cause of relapse in AML following FLT3 inhibitor treatments (3). All of the relapsed patients from AC220 treatment had acquired mutations in FLT3 that were not detected before the treatment and were confirmed to confer resistance to FLT3 inhibitors, including AC220 *in vitro*. Considering the high intrinsic genetic instability and heterogeneity of AML cells, it is now generally believed that FLT3-specific inhibitors need to be combined with other therapies to achieve the desired clinical efficacy (2). Combinations with chemotherapy have been tested with some FLT3 inhibitors like sorafenib. The combination treatments, however, have met with only moderate success primarily due to combined toxicity (6, 7).

CDK4 is a well-established cancer drug target for a broad spectrum of RB-positive cancers (23, 24). PD 0332991, a CDK4 selective inhibitor, has demonstrated clinical efficacy in treating breast cancer in combination with letrozole (17). However, CDK4 inhibition alone also faces potential clinical issue of resistance due to bypassing or compensatory mechanisms, e.g., loss of RB and increase in Cyclin E1 expression (20, 25; our unpublished observations). AMG 925 inhibits both FLT3 and CDK4 potentially offering a more effective treatment for AML than single kinase selective inhibitors. CDK4 activity is downstream of FLT3 signaling and is required for cell proliferative response to FLT3 activation. However, the function of the two kinases is not fully overlapping. As a central player in cell-cycle regulation, CDK4 mediates signaling from other upstream growth factors as demonstrated by G_1 arrest of FLT3-WT AML cells treated with AMG 925 (Fig. 1C). So, it is not surprising that inhibition of both kinases has been shown to cooperate in inhibiting AML cell growth (20). However, we hypothesize that CDK4-inhibiting activity of AMG 925 primarily acts through reducing frequency and/or expansion of mutants resistant to FLT3-inhibiting activity of the compound. Consistently, we have tried but failed to isolate AMG 925–resistant FLT3 mutations in MOLM13 and Mv4-11 under conditions that we used to isolate sorafenib-resistant mutations (our unpublished data). A potential advantage of AMG 925 over combining a FLT3 inhibitor with chemotherapy is that the CDK4-inhibiting activity of AMG 925 may be better tolerated based on the knockout phenotype of these individual targets in mice (26, 27) and clinical trial results of the CDK4 inhibitor PD 0332991 (28). AMG 925 may also be efficacious as a treatment for patients with AML refractory to or relapsed from chemotherapy.

The sequence of treatments for a combination therapy of cancer can sometimes be critical to efficacy. For example, agents causing G_1 arrest of the cell cycle are known to protect cancer cells from chemotherapies (29, 30). In contrast, it has been reported that CDK4 and FLT3 inhibitors, when added simultaneously to AML cells, acted cooperatively in inhibiting AML cell growth and inducing apoptosis (20). This result was confirmed in our experiments (our unpublished observations). Furthermore, we pretreated MOLM13 cells with CDK4 inhibitor PD 0332991 for 24 hours to arrest cells in G_1 and then determined the effect on cell proliferation of FLT3 inhibition by sorafenib. We did not detect significant effect on the sensitivity of MOLM13 to sorafenib (our unpublished observations). However, we could not exclude the possibility that longer G_1 arrest would eventually lead to decreased response to FLT3 inhibitors.

Analysis of relapsed AML in AC220-treated patients has confirmed two hot spots for resistance mutations in

Published OnlineFirst February 13, 2014; DOI: 10.1158/1535-7163.MCT-13-0858

FLT3-ITD, tyrosine kinase domain residue D835, and gatekeeper residue F691 (3). Accumulating published data suggest that FLT3 inhibitors may largely fall into two groups, one represented by AC220 and sorafenib, the other by sunitinib (31–33). The former (Type 2) are much less active on FLT3-ITD/D835 and FLT3-ITD-F691 mutations, whereas the latter (Type 1) is less affected by these mutations. As an FLT3 kinase inhibitor, AMG 925 seems to fall into the Type 1 group as it inhibits sorafenib-resistant FLT3-ITD-D835Y/V mutations. In addition, our preliminary unpublished results showed that AMG 925 similarly inhibited FLT3-ITD-D835Y and -F691I in BaF3 cells. Several kinase inhibitors with similar inhibition profiles of FLT3-mutant inhibition have been reported for having a potential to overcome AC220 resistance (34, 35). Inhibition of resistance mutations at residues D835 and F691 by AMG 925 would present a tempting option to combine with the Type 1 inhibitors AC220/sorafenib to enhance efficacy in treating AML.

In summary, mutational resistance has been a clinical issue of FLT3 inhibitors as monotherapy and combination therapies are being pursued. We have demonstrated AMG 925 in preclinical systems to be a potent, selective, and orally bioavailable FLT3/CDK4 dual kinase inhibitor. The compound demonstrated *in vivo* activity in AML tumor models and seemed well tolerated. AMG 925 is currently at the late stage of preclinical development. Future clinical testing will determine the efficacy of the compound in treating FLT3-mutant AML for its potential to cause a durable clinical response.

Disclosure of Potential Conflicts of Interest

J.C. Medina and A. Kamb have ownership interest in Amgen, Inc. No potential conflicts of interest were disclosed by the other authors.

Authors' Contributions

Conception and design: K. Keegan, Z. Li, M. Ragains, X. Wang, C. Quéva, L.R. McGee, J. Medina, A. Kamb, D. Wickramasinghe, K. Dai
Development of methodology: K. Keegan, C. Li, M. Ragains, J. Huard, L. Liu, J. Medina, K. Dai
Acquisition of data (provided animals, acquired and managed patients, provided facilities, etc.): K. Keegan, C. Li, J. Ma, S. Coberly, D. Hollenback, M. Weidner, J. Huard, G. Alba, J. Orf, M.-C. Lo, S. Zhao, R. Ngo, A. Chen, T. Carlson
Analysis and interpretation of data (e.g., statistical analysis, biostatistics, computational analysis): K. Keegan, J. Ma, S. Coberly, J. Eksterowicz, J. Huard, J. Orf, S. Zhao, T. Carlson, D. Wickramasinghe, K. Dai
Writing, review, and/or revision of the manuscript: K. Keegan, M. Ragains, S. Coberly, D. Hollenback, J. Eksterowicz, J. Huard, G. Alba, M.-C. Lo, S. Zhao, L. Liu, T. Carlson, L.R. McGee, J. Medina, A. Kamb, D. Wickramasinghe, K. Dai
Administrative, technical, or material support (i.e., reporting or organizing data, constructing databases): K. Keegan, L. Liang, J. Huard, J. Medina, A. Kamb
Study supervision: K. Keegan, J. Ma, C. Quéva, D. Wickramasinghe, K. Dai

Acknowledgments

The authors thank Tammy L. Bush and Michelle DuPont for carrying out the study in the Colo205 xenomouse tumor model. They also thank Wes Chang and Jay Danno at Amgen Clinical Immunology for performing the flow cytometry and Tammy L. Bush and Gene Cutler for critical reading of the article.

The costs of publication of this article were defrayed in part by the payment of page charges. This article must therefore be hereby marked *advertisement* in accordance with 18 U.S.C. Section 1734 solely to indicate this fact.

Received October 9, 2013; revised January 20, 2014; accepted February 4, 2014; published OnlineFirst February 13, 2014.

References

1. American Cancer Society. Cancer Facts & Figures 2014. Atlanta: American Cancer Society; 2014. http://www.cancer.org.
2. Kayser S, Levis MJ. FLT3 tyrosine kinase inhibitors in acute myeloid leukemia: clinical implications and limitations. Leuk Lymphoma 2014;55:243–55.
3. Smith CC, Wang Q, Chin CS, Salerno S, Damon LE, Levis MJ, et al. Validation of ITD mutations in FLT3 as a therapeutic target in human acute myeloid leukaemia. Nature 2012;485:260–3.
4. Kindler T, Lipka DB, Fischer T. FLT3 as a therapeutic target in AML: still challenging after all these years. Blood 2010;116:5089–102.
5. Grunwald MR, Levis M. FLT3 inhibitors for acute myeloid leukemia: a review of their efficacy and mechanisms of resistance. J Int J Hematol 2013;97:683–94.
6. Al-Kali A, Cortes J, Faderl S, Jones D, Abril C, Pierce S, et al. Patterns of molecular response to and relapse after combination of sorafenib, idarubicin, and cytarabine in patients with FLT3 mutant acute myeloid leukemia. Clin Lymphoma Myeloma Leuk 2011;11:361–6.
7. Stone RM, Fischer T, Paquette R, Schiller G, Schiffer CA, Ehninger G, et al. Phase IB study of the FLT3 kinase inhibitor midostaurin with chemotherapy in younger newly diagnosed adult patients with acute myeloid leukemia. Leukemia 2012;26:2061–8.
8. Malumbres M, Barbacid M. To cycle or not to cycle: a critical decision in cancer. Nat Rev Cancer 2001;1:222–31.
9. Kamb A, Gruis NA, Weaver-Feldhaus J, Liu Q, Harshman K, Tavtigian SV, et al. A cell cycle regulator potentially involved in genesis of many tumor types. Science 1994;264:436–40.
10. Serrano M, Hannon GJ, Beach D. A new regulatory motif in cell-cycle control causing specific inhibition of cyclin D/CDK4. Nature 1993;366:704–7.
11. Weinberg RA. The retinoblastoma gene and cell growth control. Trends Biochem Sci 1990;15:199–202.
12. Lee WH, Shew JY, Hong FD, Sery TW, Donoso LA, Young LJ, et al. The retinoblastoma susceptibility gene encodes a nuclear phosphoprotein associated with DNA binding activity. Nature 1987;329:642–5.
13. Ortega S, Malumbres M, Barbacid M. Cyclin D-dependent kinases, INK4 inhibitors and cancer. Biochim Biophys Acta 2002;1602:73–87.
14. Matsuno N, Hoshino K, Nanri T, Kawakita T, Suzushima H, Kawano F, et al. p15 mRNA expression detected by real-time quantitative reverse transcriptase-polymerase chain reaction correlates with the methylation density of the gene in adult acute leukemia. Leuk Res 2005;29:557–64.
15. Drexler HG. Review of alterations of the cyclin-dependent kinase inhibitor INK4 family genes p15, p16, p18 and p19 in human leukemia-lymphoma cells. Leukemia 1998;12:845–59.
16. Fry DW, Harvey PJ, Keller PR, Elliott WL, Meade M, Trachet E, et al. Specific inhibition of cyclin-dependent kinase 4/6 by PD 0332991 and associated antitumor activity in human tumor xenografts. Mol Cancer Ther 2004;3:1427–38.
17. Finn RS, Crown JP, Lang I, Boer K, Bondarenko IM, Kulyk SO, et al. Results of a randomized phase 2 study of PD 0332991, a cyclin-dependent kinase (cdk) 4/6 inhibitor, in combination with letrozole vs letrozole alone for first-line treatment of ER+/HER2- advanced breast cancer. Cancer Res (Supplement) 2012;72:1s–608s (Abstract, 2012 San Antonio Breast Cancer Symposium).
18. Baughn LB, Di Liberto M, Wu K, Toogood PL, Louie T, Gottschalk R, et al. A novel orally active small molecule potently induces G1 arrest in primary myeloma cells and prevents tumor growth by specific inhibition of cyclin-dependent kinase 4/6. Cancer Res 2006;66:7661–7.

Published OnlineFirst February 13, 2014; DOI: 10.1158/1535-7163.MCT-13-0858

19. Leonard JP, LaCasce AS, Smith MR, Noy A, Chirieac LR, Rodig SJ, et al. Selective CDK4/6 inhibition with tumor responses by PD0332991 in patients with mantle cell lymphoma. Blood 2012;119:4597–607.
20. Wang L, Wang J, Blaser BW, Duchemin AM, Kusewitt DF, Liu T, et al. Pharmacologic inhibition of CDK4/6: mechanistic evidence for selective activity or acquired resistance in acute myeloid leukemia. Blood 2007;110:2075–83.
21. Bose P, Simmons GL, Grant S. Cyclin-dependent kinase inhibitor therapy for hematologic malignancies. Expert Opin Investig Drugs 2013;22:723–38.
22. Choudhary C, Brandts C, Schwable J, Tickenbrock L, Sargin B, Ueker A, et al. Activation mechanisms of STAT5 by oncogenic Flt3-ITD. Blood 2007;110:370–4.
23. Malumbres M, Barbacid M. Is cyclin D1-CDK4 kinase a bona fide cancer target? Cancer Cell. 2006;9:2–4.
24. Musgrove EA, Caldon CE, Barraclough J, Stone A, Sutherland RL. Cyclin D as a therapeutic target in cancer. Nat Rev Cancer 2011;11:558–72.
25. Dean JL, Thangavel C, McClendon AK, Reed CA, Knudsen ES. Therapeutic CDK4/6 inhibition in breast cancer: key mechanisms of response and failure. Oncogene 2010;29:4018–32.
26. Satyanarayana A, Kaldis P. Mammalian cell-cycle regulation: several Cdks, numerous cyclins and diverse compensatory mechanisms. Oncogene 2009;28:2925–39.
27. Lee YM, Sicinski P. Targeting cyclins and cyclin-dependent kinases in cancer: lessons from mice, hopes for therapeutic applications in human. Cell Cycle 2006;5:2110–4.
28. Flaherty KT, Lorusso PM, Demichele A, Abramson VG, Courtney R, Randolph SS, et al. Phase I, dose-escalation trial of the oral cyclin-dependent kinase 4/6 inhibitor PD 0332991, administered using a 21-day schedule in patients with advanced cancer. Clin Cancer Res 2012;18:568–76.
29. Stone S, Dayananth P, Kamb A. Reversible, p16-mediated cell cycle arrest as protection from chemotherapy. Cancer Res 1996;56:3199–202.
30. McClendon AK, Dean JL, Rivadeneira DB, Yu JE, Reed CA, Gao E, et al. CDK4/6 inhibition antagonizes the cytotoxic response to anthracycline therapy. Cell Cycle. 2012;11:2747–55.
31. von Bubnoff N, Engh RA, Aberg E, Sänger J, Peschel C, Duyster J. FMS-like tyrosine kinase 3-internal tandem duplication tyrosine kinase inhibitors display a nonoverlapping profile of resistance mutations in vitro. Cancer Res 2009;69:3032–41.
32. Moore AS, Faisal A, Gonzalez de Castro D, Bavetsias V, Sun C, Atrash B, et al. Selective FLT3 inhibition of FLT3-ITD+ acute myeloid leukaemia resulting in secondary D835Y mutation: a model for emerging clinical resistance patterns. Leukemia 2012;26:1462–70.
33. Kancha RK, Grundler R, Peschel C, Duyster J. Sensitivity toward sorafenib and sunitinib varies between different activating and drug-resistant FLT3-ITD mutations. Exp Hematol 2007;35:1522–6.
34. Farrell P, Shi L, Matuszkiewicz J, Balakrishna D, Hoshino T, Zhang L, et al. Biological characterization of TAK-901, an investigational, novel, multitargeted Aurora B kinase inhibitor. Mol Cancer Ther 2013;12:460–70.
35. Kesarwani M, Huber E, Azam M. Overcoming AC220 resistance of FLT3-ITD by SAR302503. Blood Cancer J. 2013;3:e138.

Published OnlineFirst February 13, 2014; DOI: 10.1158/1535-7163.MCT-13-0858

Molecular Cancer Therapeutics

Preclinical Evaluation of AMG 925, a FLT3/CDK4 Dual Kinase Inhibitor for Treating Acute Myeloid Leukemia

Kathleen Keegan, Cong Li, Zhihong Li, et al.

Mol Cancer Ther 2014;13:880-889. Published OnlineFirst February 13, 2014.